We are IntechOpen, the world's leading publisher of Open Access books
Built by scientists, for scientists

4,800
Open access books available

122,000
International authors and editors

135M
Downloads

154
Countries delivered to

Our authors are among the

TOP 1%
most cited scientists

12.2%
Contributors from top 500 universities

CLARIVATE ANALYTICS
BOOK CITATION INDEX
INDEXED

WEB OF SCIENCE™

Selection of our books indexed in the Book Citation Index
in Web of Science™ Core Collection (BKCI)

Interested in publishing with us?
Contact book.department@intechopen.com

Numbers displayed above are based on latest data collected.
For more information visit www.intechopen.com

Tensile Strength of Unidirectional Carbon Fiber-Reinforced Plastic Composites

Go Yamamoto, Keita Koizumi and Tomonaga Okabe

Abstract

The tensile strengths of unidirectionally aligned carbon fiber-reinforced plastic (UD-CFRP) were predicted by implementing a spring element model (SEM) that takes into account a stress concentration acting on an intact fiber surface originated from a fracture site in an neighboring fiber. The surface stress concentration was experimentally investigated by implementing multi-fiber fragmentation testing in combination with the SEM simulation. Four types of epoxy materials were selected to explore the effects of matrix polymer properties on the surface stress concentration. The size scaling results, coupled with the results of the SEM simulation, designed to take into account the surface stress concentration, were reasonably consistent with the experimentally obtained data on the tensile strengths of the UD-CFRP composites, irrespective of the differences in the matrix mechanical characteristics. The possible mechanisms by which additional stress concentration is generated on an intact fiber surface were analyzed numerically using the finite element method.

Keywords: carbon fiber-reinforced plastic (CFRP), tensile strength prediction, fiber fragmentation, stress concentrations, finite element analysis

1. Introduction

Tensile strength prediction of unidirectional carbon fiber-reinforced plastic (UD-CFRP) composites had been one of the major topics of CFRP composite research since the 1950s. Many attempts had been conducted to predict tensile strength, including the early pioneering work by Cox [1], Rosen [2], and Kelly and Tyson [3]. In recent years the studies using enhanced computer simulations have deepened the understanding of failure processes of a UD-CFRP composite, and these studies have enabled greatly increased understanding of the failure of the composite structures [4, 5]. More recently the work by Swolfs and colleagues showed observations of individual fiber breaks occurring leading to the creation of clusters of breaks in UD-CFRP composites using high-resolution synchrotron tomography, leading to an experimental proof of critical cluster size [4]. The work by Thionnet and colleagues has used a 3D multi-scale simulation coupled with experimental results which has allowed a detailed understanding of failure in UD-CFRP composites including the kinetics of fiber breaks not only in monotonic tests but also in long-term steady load tests [5]. Moreover, improved computer

techniques have enriched the understanding of the failure processes of UD-CFRP composites [4–7].

According to the above-mentioned previous reports, the failure mechanisms of UD-CFRP composites can be described as follows: no load perturbation resulting from a fiber break is uniformly distributed among the surviving fibers because it is more heavily applied to the next fibers. Therefore, when a fiber breaks, the load that it is carrying is transferred to the surviving neighbors, increasing the degree of concentrated stress on these fibers relative to more distant fibers and increasing the probability of failure at this position. This consequently leads to the constitution of broken fiber clusters and subsequent failure of the UD-CFRP composites. Considering such fracture processes, although a large number of studies have only addressed the load redistribution caused by fiber breakage, several studies that have implemented fragmentation tests have reported that a matrix crack or damage to a matrix comes from around a fiber break point. Although the concentrated stress on an intact fiber surface neighboring a fiber break point has been widely acknowledged as a critical factor determining the ultimate tensile strength of UD-CFRP composites, the strength prediction of such composite considering the stress concentration owing to the fiber failure is so far from satisfactory.

Here we considered the stress concentration acting on an intact fiber surface caused by a fracture site in a neighboring broken fiber into our prediction of the ultimate tensile strengths of the UD-CFRP composites. The concentrated stress acting on the intact fiber surface was investigated by utilizing a double-fiber fragmentation testing in combination with a SEM simulation. The acquired stress concentration factors were then implemented to access the tensile strength of the UD-CFRP composites. The double-fiber fragmentation composites and the UD-CFRP composites were elaborated with a T1100G-type carbon fiber and epoxy material and tested to validate the proposed prediction method. The size scaling results obtained in conjunction with the results obtained from the SEM simulation were reasonably consistent with the experimental data on the tensile strengths of the UD-CFRP composites. We have also systematically investigated a possible scenario on the origin of stress concentrations generated on an intact fiber surface which is investigated through a numerical analysis based on the finite element method.

2. Experimental method

2.1 Sample preparation and mechanical characterization

T1100G-type carbon fiber and four types of bisphenol-A-epoxy resin materials were used to elaborate multi-fiber and UD-CFRP composites. The four types of preheated and degassed epoxy resins were separately poured into a preheated glass mold, then cured in an air oven at 160°C for 5 h followed by post-curing at 180°C for 2 h. The specimens were cut into a dumbbell shape (gauge length = 30 mm; width narrow parallel portion = 5 mm; thickness = 1 mm) according to the JIS-K7161-2 standard. The mechanical properties were measured by uniaxial tensile loading tests performed on a servohydraulic testing machine (i.e., MTS Landmark) with a loading cell of 50 kN under atmospheric conditions at room temperature. The load application was performed at a crosshead speed of 4.17 μm/s (0.25 mm/min). Two strain gauges were mounted along the longitudinal and transverse directions on the sample. **Figure 1** indicates that tensile loading experiments performed herein revealed that the four types of epoxy materials exhibited different mechanical characteristics. Therefore, the epoxy materials are hereafter referred to as
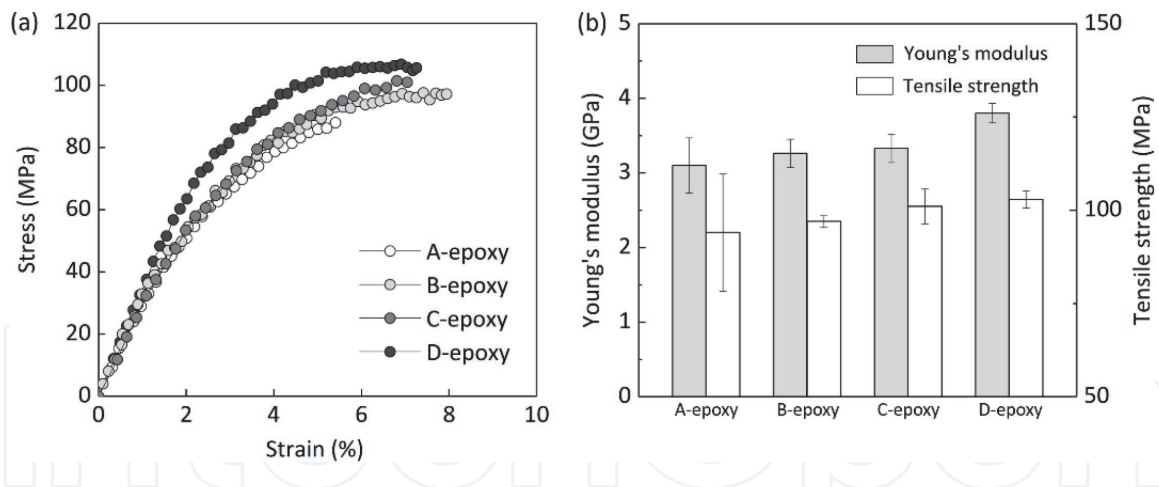
Figure 1.
Summary of the (a) stress–strain curves and (b) mechanical properties for the four types of epoxy materials.

"A-epoxy," "B-epoxy," "C-epoxy," and "D-epoxy," with the order of the names indicating the magnitude of the elastic modulus.

Multi-fiber fragmentation specimens were elaborated by positioning two to four fibers parallel to the loading direction, implementing an interfiber spacing of approximately one-half to four fiber diameters (i.e., approximately 3.5–20.0 μm). The details of sample preparation can be found in [8]. Multi-fiber fragmentation tests were conducted to facilitate the derivation of a quantitative description of fiber failure mechanisms by using a polarized light microscope equipped with a four-point bending machine. A strain gauge was used to monitor the tensile strain applied to the fibers. The tensile strain was increased in 0.1% steps until a maximum of 5.0% strain was applied and kept constant during the measurement of both the number and positions of the broken fibers. The number of fractured fibers observed under the pure bending conditions was measured using the microscope. The strain applied to the fiber ε_f was calculated as follows:

$$\varepsilon_f = \varepsilon_c \times \frac{2.0}{\kappa} \times \left(\frac{t - 2d}{t} \right) - \varepsilon_f^r, \tag{1}$$

where ε_c is the acquired composite strain, κ is the gauge factor (=2.13), t is the thickness of the multi-fiber specimens (=~2 mm), d is the embedded fiber depth (=~60 μm), and ε_f^r is the indirectly applied strain that comes from the included residual strain on the fiber caused by the thermal expansion mismatch between them. The tensile strengths of the UD-CFRP composites were investigated to validate the accuracy of the predicted tensile strength. The composites were elaborated via conventional technique to prepare the laminate structure of $[0_6]$. The volume fraction of the fiber and the density of the UD-CFRP composites were 57% and 1.79 Mg/m^3, respectively. The tensile strength of the composites was measured via tensile loading tests under ambient conditions. The crosshead speed and the gauge length were 21.2 μm/s (1.27 mm/min) and 127 mm, respectively.

2.2 Model preparation

Monte Carlo methods were mounted in the SEM simulation to investigate the SCF on the intact fiber surface next to the fiber break points. The details of model preparation and simulation procedures can be found in [8]. In brief, a simulation model consisted of longitudinal and transverse spring in a 3D hexagonal arrangement. In this analysis, the longitudinal elements behave as carbon fibers that exclusively sustain the tensile load, while the transverse elements work as a matrix that

only carries the shearing load. The stiffness matrices of the fiber matrix elements are separately calculated as follows:

$$K_L^e = \pi R^2 \int_0^l B_L^{eT} E_f B_L^e \, dz, \tag{2}$$

$$K_T^e = \frac{\pi R l}{3} \int_0^l B_T^{eT} G_m B_T^e \, dr, \tag{3}$$

$$B_L^e = \begin{bmatrix} \frac{1}{l} & -\frac{1}{l} \end{bmatrix}, \tag{4}$$

$$B_T^e = \begin{bmatrix} \frac{1}{d} & -\frac{1}{d} \end{bmatrix}, \tag{5}$$

where K_L^e and K_T^e are the stiffness matrices of the fiber and matrix elements, respectively. Subscripts L and T represent the longitudinal and transverse spring elements, respectively, E_f is the Young's modulus of the fiber (=324 GPa), G_m is the shear modulus of a matrix (=1.4 GPa), R is the radius of the fiber (=2.7 μm), and l and d are the element lengths along the longitudinal and transverse directions, respectively. The length of the transverse spring d can be obtained as follows:

$$d = \begin{cases} 0.01 & (f \leq 4) \\ R\left(\sqrt{\dfrac{2\pi}{\sqrt{3}V_f}} - 2 \right) & (f > 4) \end{cases}, \tag{6}$$

where V_f and f are the volume fraction of the fiber (= 57%) and the number of fibers in the SEM, respectively. The experimentally acquired average interfiber spacing in the multi-fiber fragmentation specimens was ∼0.01 mm. Therefore, d was set to 0.01 to examine the results of the multi-fiber fragmentation tests conducted under the condition that the maximum number of fibers in the model is four. A hexagonal close-packed structure was assumed for the analysis of the full composite model. In the SEM having two to four fibers, the longitudinal elements other than the fibers are assigned as a matrix; therefore, the stiffness of a matrix is implemented in the longitudinal elements.

With the aim of simplicity, the SEM model considers exclusively the effect of plastic deformation of the matrix. The axial stress σ_s in the broken fiber when plastic deformation occurs in the matrix close to the fiber breaking point or the fiber edge is expressed as a function of distance D_s from those positions as follows:

$$\sigma_s = \frac{2\tau_s D_s}{R}, \tag{7}$$

where τ_s is the interfacial shear stress and is postulated to be constant; the matrix behaves as an elasto-perfectly plastic body, and the equilibrium equation to represent the entire system is given as follows:

$$\left[\sum_{e=1}^{N_f - N_b - N_p} K_L^e - \sum_{e=1}^{N_m} K_T^e \right] u + \sum_{e=1}^{N_p} \pi R^2 \int_0^l B_L^{eT} \sigma_s \, dz = f, \tag{8}$$

where N_f and N_m are the number of spring elements for the fiber and matrix, respectively, N_b is the number of fractured fibers, and N_p is the number of fiber spring elements in the plastic deformation region. We considered herein the

situation where the fiber failure is assumed to take place at the fiber surface, based on the fact that almost all fibers were broken by surface flaws [9]. Therefore, the probability of fiber breakage $P_f(\sigma)$ under the condition that the fiber is subjected to stress σ at the surface area $S_f \ (= 2\pi RL_f)$ is given as follows:

$$P_f(\sigma) = 1 - \exp\left\{ -\frac{S_f}{S_{f,0}}\left(\frac{\sigma}{\sigma_{01}}\right)^{m_1} - \frac{S_f}{S_{f,0}}\left(\frac{\sigma}{\sigma_{02}}\right)^{m_2} \right\}, \qquad (9)$$

where $S_{f,0} \ (= 2\pi RL_{f,0})$ is the fiber surface area ($L_{f,0}$ = 10 mm), L_f is the gauge length, σ_{01} (=7.7) and σ_{02} (=9.1) are the Weibull scale parameters, and m_1 (=4.5) and m_2 (=13.0) are the Weibull shape parameters. The details of the Weibull parameter determination procedures can be found in [10, 11]. Fibers are hexagonally arranged in the model; thus, the fiber surface can be divided into six parts. Thus, taking into account the contribution of concentrated stress acting an intact fiber surface, the probability of fiber breakage $P_{f,i}$ (σ) can be rewritten as follows:

$$P_{f,i}(\sigma) = 1 - \exp\left\{ -\frac{S_{f,i}}{S_{f,0}}\left(\frac{\alpha_i\sigma}{\sigma_{01}}\right)^{m_1} - \frac{S_{f,i}}{S_{f,0}}\left(\frac{\alpha_i\sigma}{\sigma_{02}}\right)^{m_2} \right\}, \qquad (10)$$

where $S_{f,i}$ is the i-th fiber segment of the surface area ($S_{f,i} = \pi RL_{f,0}/3$). The SEM does not represent the matrix aside from the shear load directly. Thus, the additional stress concentration is applied in an ad hoc manner to illustrate the experimentally observed correlations in fiber failures. The strength of the n-th fiber segment is determined by choosing a random number R_n ranging from 0 to 1 and solving equation $R_n = P_{f,n}(\sigma)$. The longitudinal spring element was removed from the simulation model when the stress applied to a fiber at the n-th fiber segment achieved the statistical distribution of the strength of the fiber σ_n.

The surface SCFs α of an intact fiber were investigated by implementing the SEM to investigate the α value, with the purpose of ensuring that it was equivalent to the coordinated fracture percentage, which is defined as a failure occurring at the elements adjacent to a broken element in the same horizontal plane of the broken fiber element that was determined via multi-fiber-fiber fragmentation testing. Thus, the two to four longitudinal elements in the center of the SEM were assigned to the fibers, and the remaining were assigned to the matrix. In the study, the bimodal Weibull distribution was implemented as the statistical distribution of fiber strength. The full composite model comprised 1024 fibers measuring 3 mm in length that were divided into 300 segments. Prior to comparing the simulated results to the experimental data, the simulated strengths were subjected to size scaling [12].

3. Results and discussion

First, the UD-CFRP composites made with four types of matrix polymers were elaborated and then employed with tensile loading tests to investigate their mechanical properties along the direction of the fiber axis. As shown in **Figure 2**, all composites tested in this study demonstrated catastrophic failure after reaching a maximum load, exhibiting a stress–strain relationship that is typically observed in conventional UD-CFRP composites; no clear difference was noted between the Young's modulus values, whereas, for example, the composite fabricated with the D-epoxy demonstrated strength enhanced by a factor of about 1.2 compared to the composite prepared with the A-epoxy.
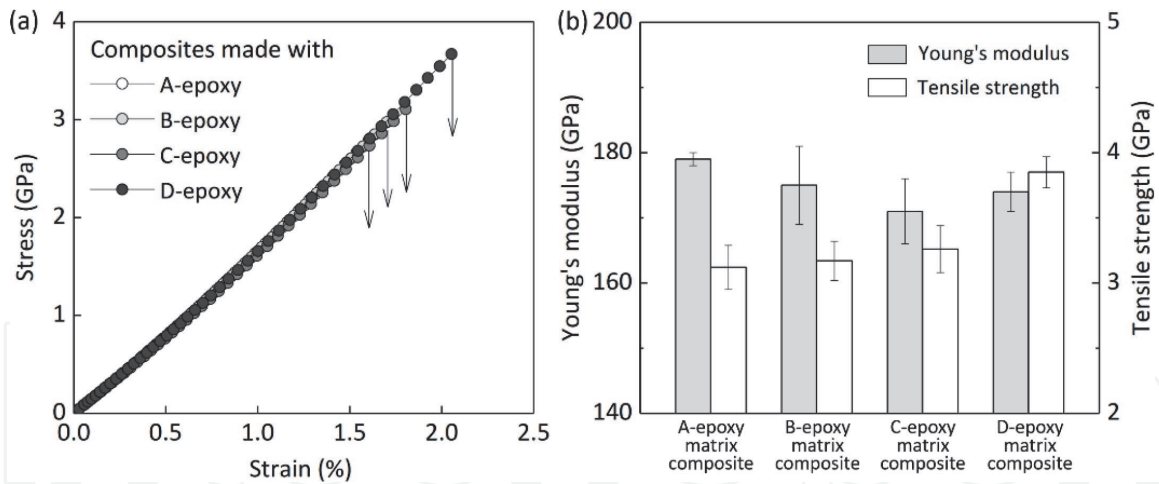
Figure 2.
Summary of the (a) stress–strain curves and (b) mechanical properties for the four types of UD-CFRP composites.

As previously mentioned, the fibers next to a broken fiber were applied to enhanced concentrated stress, leading to the increased of the failure probability. Thus, the understanding of the failure processes of the above-mentioned fiber is a requirement for the tensile strength prediction of UD-CFRP composites. A double-fiber fragmentation testing was conducted in order to investigate the effects of the interfiber spacing on the failure processes of such fibers. First, the B-epoxy was used in the specimen preparation. It was found from the double-fiber fragmentation testing that a large number of fiber underwent failure at similar positions, suggesting that the concentrated stress generated by fiber failure was sufficiently high to cause the next fiber to fracture, which nullifies the influence of randomly distributed flaws along the fiber on the fiber strength. The percentages of coordinate fractures observed for the double-fiber composites with interfiber spacings of 3.6, 9.9, and 20.0 μm were 73, 57, and 60%, respectively. Even though some flocculation has been observed for the percentages of coordinate fractures, the acquired percentages appeared to be higher than those observed for fiber failure that was governed by the statistical strength distribution of fibers [13]. This indicates that for an interfiber spacing of one-half to four fiber diameters, the failure processes of the fiber were governed by the fiber-fiber interactions.

Next, the fiber fracture behavior of the multi-fiber fragmentation specimens having up to four fibers was investigated to determine the surface SCFs. The microscopy observation revealed that matrix cracks and the coordination of fractures in neighboring fibers have been observed in multi-fiber fragmentation specimens, irrespective of the number of fibers. The coordinated fracture percentages in the double-fiber specimens tended to increase as the number of fibers was increased. At 3.2% fiber strain (i.e., ε_f calculated via Eq. (1) for a composite strain εc of 5.0%), the coordinated fracture percentages in the double-, triple-, and quadruple-fiber specimens were calculated to be 48.3% ($\pm$14.1%), 33.3% ($\pm$17.8%), and 15.8% ($\pm$5.8%), respectively.

A quantitative determination of the surface SCFs α on an intact fiber next to a fiber break point was achieved by implementing the SEM to investigate the α. **Figure 3a** shows the relationship between the SCF and the coordinated fracture percentages for each fragmentation specimen, which was determined by systematically sweeping α in the SEM simulation. The simulation results demonstrated that the percentages increased with an increased SCF and decreased in response to an increase in the number of fibers. By comparing the simulated coordinated fracture percentages to the experimentally obtained data, the surface SCF on an intact fiber
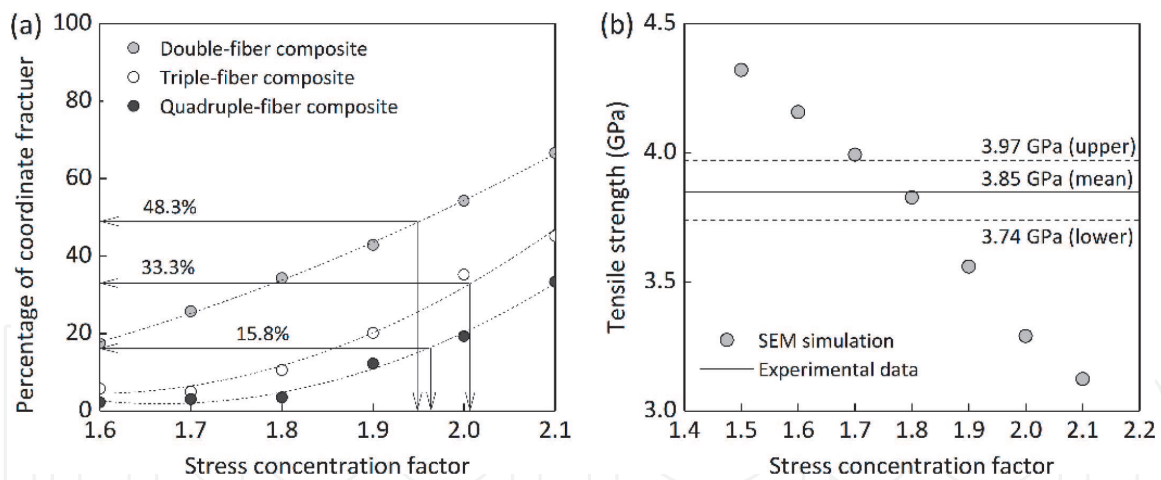
Figure 3.
(a) Relationship between the stress concentration factors and the percentage of coordinated fractures. (b) Experimental and simulated results for the UD-CFRP composites.

appeared to be ∼2.0. Furthermore, no fiber number significantly affects the surface SCF, suggesting that for the UD-CFRP composites elaborated with the B-epoxy, the stress concentration acting on the fiber surface was approximately twice as much as the fiber stress with no additional surface stress concentration. **Figure 3b** depicts a comparison of the simulated experimental results for the UD-CFRP composites prepared with the B-epoxy. As indicated in **Figure 3b**, the measured tensile strengths of the B-epoxy matrix composites are 3.05–3.32 GPa (mean, 3.17 GPa). The simulated data that acquired no consideration of the added concentrated stress were incongruent with the experimental data, whereas the predictions incorporating an SCF of 2.0 were reasonably consistent with the experimental data, indicating that the prediction method proposed herein yields a reasonably accurate tensile strength prediction when the matrix crack-induced surface stress concentration of fibers is appropriately considered.

We implemented the above-mentioned strength prediction method into the UD-CFRP composites elaborated with the "A-epoxy," "C-epoxy," and "D-epoxy." The surface SCF on intact fibers was acquired via the double-fiber fragmentation testing taking into account of the fact that for the B-epoxy matrix composites, no fibers number influence the SCFs. The SCFs were calculated as ∼2.15 for the A-epoxy material, ∼1.93 for the C-epoxy material, and ∼1.75 for the D-epoxy material. Thus, surface SCFs were implemented to access the tensile strength of the three types of the UD-CFRP composite materials. In one example, as shown in **Figure 2b**, the measured tensile strengths of the D-epoxy matrix composites ranged from 3.74 to 3.97 GPa (mean, 3.85 GPa). The estimated tensile strength simulated under the condition of $\alpha = 1.75$ was ∼3.9 GPa. Consequently, the results demonstrate that, even if the mechanical properties of the matrix materials vary, the proposed method can yield a reasonable prediction of the tensile strength of the UD-CFRP composites.

The possible mechanisms by which the additional concentrated stress occurs is not clear so far; moreover it is unclear why the SCF varies depending on the matrix mechanical properties. A numerical analysis using the FEM was performed to understand possible mechanisms by which significant stress occurred on the intact fiber surface next to the fiber break point. The details of model preparation and material properties can be found in [8]. In brief, a hexagonal fiber arrangement was used in this study, and only one-half of the composite structure was modeled and analyzed due to reasons of structural symmetry. The plasticity-free layer model, referred to as the SSV model [10], an elastic layer with a thickness of 50 nm, was
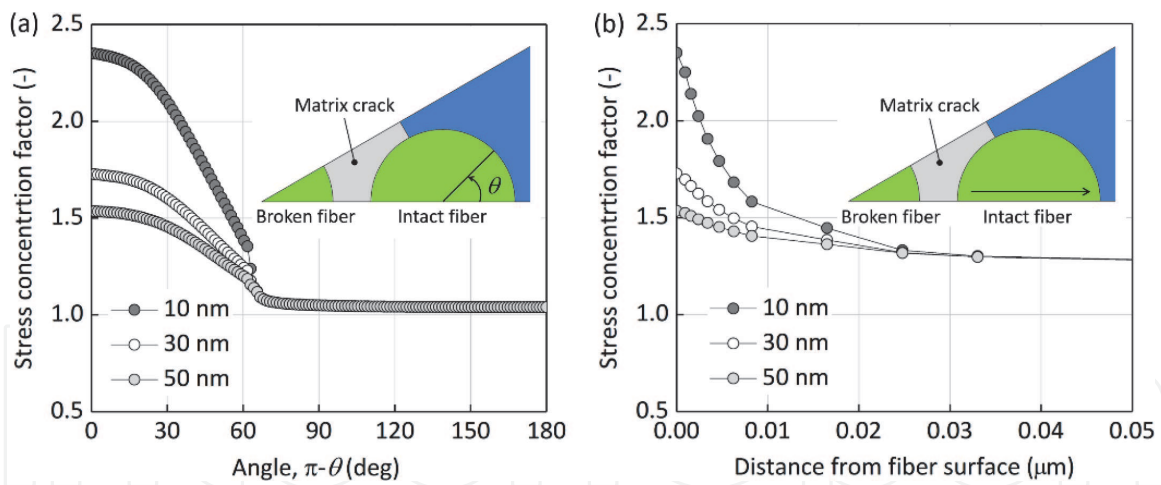
Figure 4.
Positional dependence of the SCF in the (a) circumferential direction and (b) diameter direction of the intact fiber.

applied around the matrix crack using the same elastic properties as the D-epoxy material. No matrix crack was assumed to reach the intact fiber surface, and there was a gap between the crack tip and the intact fiber surface. In this analysis, the gap was changed to 10, 30, and 50 nm. The elastic stiffnesses of the T1100G-type carbon fiber are listed in [11].

It was demonstrated that an SCF of α = ~1.7, as observed for the D-epoxy matrix composite with the gap of 30 nm, was indeed on the surface of the intact fiber. Here, the SCF was defined as the ratio of the stress of an outermost surface element of the intact fiber to the stress in an element sufficiently away from the fiber break point. Note that the stress recovery behavior in the broken fiber was reasonably consistent with that obtained from the SEM simulation under the SCF condition of α = 1. **Figure 4a** shows the effects of the gap on the SCF in the circumferential direction of the intact fiber; the SCF decreases with the increase in the measurement angle, and the SCF reaches almost 1, regardless of the differences in the gaps. **Figure 4b** summarizes the effects of the gap on the SCF in the diameter direction of the intact fiber; the SCF decreases with the increase in the distance from fiber surface, indicating that a significantly higher stress concentration is generated on the outermost surface area, and the degree of stress concentration is going to be small rapidly inside the fiber. The averaged SCF subjecting on the full cross-sectional area of the intact fiber next to a broken fiber at the plane of fracture was calculated to be approximately 1.1. This "averaged SCF" is reasonably consistent with the previously reported averaged SCF around a broken fiber in a UD-CFRP composite [14–17].

4. Conclusions

Four types of UD-CFRP composite materials with different mechanical characteristics were elaborated in this study. The tensile strengths of the fabricated composites were predicted via a SEM simulation based on the results obtained from multi-fiber fragmentation experiments. The primary aim of this study was to explore the effects of matrix polymer properties on the stress concentrated on the fiber surface. It was revealed that the extent of concentrated stress acting on the intact fiber surface can be changed by modifying the mechanical properties of the matrix polymer. By employing an epoxy matrix having a higher Young's modulus

and increased tensile strength in the composite preparation reduced the SCF from a $\sim$2.15 to $\sim$1.75. We have also shown a numerical scenario on the origin of the stress concentrations that are generated on the intact fiber surface by implementing the SSV model and employing the rehardening characteristics of epoxy materials. Finally, we confirmed that employing the measured SCFs and bimodal Weibull distribution to determine how strength is statistically distributed throughout the fiber yields the predicted strengths of the four types of UD-CFRP composites that are reasonably consistent with the experimental data, thereby demonstrating the validity of the proposed prediction method.

Acknowledgements

Author details

Go Yamamoto*, Keita Koizumi and Tomonaga Okabe
Department of Aerospace Engineering, Tohoku University, Sendai, Japan

*Address all correspondence to: yamamoto@plum.mech.tohoku.ac.jp

IntechOpen

References

[1] Cox HL. The elasticity and strength of paper and other fibrous materials. British Journal of Applied Physics. 1952;**3**(3):72-79. DOI: 10.1088/0508-3443/3/3/302

[2] Rosen BW. Tensile failure of fibrous composites. AIAA Journal. 1964;**2**(11): 1985-1991. DOI: 10.2514/3.2699

[3] Kelly A, Tyson W. Tensile properties of fibre-reinforced metals: Copper/ tungsten and copper/molybdenum. Journal of the Mechanics and Physics of Solids. 1965;**13**(6):329-350

[4] Swolfs Y, Morton H, Scott AE, Gorbatikh L, Reed PAS, Sinclair I, et al. Synchrotron radiation computed tomography for experimental validation of a tensile strength model for unidirectional fibre-reinforced composites. Composites Part A Applied Science and Manufacturing. 2015;**77**(6): 106-113. DOI: 10.1016/j. compositesa.2015.06.018

[5] Thionnet A, Chou HY, Bunsell A. Fiber break processes in unidirectional composites. Composites Part A Applied Science and Manufacturing. 2014;**65**: 148-160. DOI: 10.1016/j. compositesa.2014.06.009

[6] Chou HY, Bunsell AR, Mair G, Thionnet A. Effect of the loading rate on ultimate strength of composites. Application: Pressure vessel slow burst test. Composite Structures. 2013;**104**: 144-153. DOI: 10.1016/j. compstruct.2013.04.003

[7] Tavares RP, Otero F, Turon A, Camanho PP. Effective simulation of the mechanics of longitudinal tensile failure of unidirectional polymer composites. International Journal of Fracture. 2017; **208**(1–2):269-285. DOI: 10.1007/ s10704-017-0252-9

[8] Yamamoto G, Onodera M, Koizumi K, Watanabe J, Okuda H, Tanaka F, et al. Considering the stress concentration of fiber surfaces in the prediction of the tensile strength of unidirectional carbon fiber-reinforced plastic composites. Composites Part A Applied Science and Manufacturing. 2019;**121**:499-509. DOI: 10.1016/j. compositesa.2019.04.011

[9] Watanabe J, Tanaka F, Higuchi R, Matsutani H, Okuda H, Okabe T. A study of stress concentrations around fiber breaks in unidirectional CF/epoxy composites using double-fiber fragmentation tests. Advanced Composite Materials. 2018;**27**(6): 575-587. DOI: 10.1080/ 09243046.2017.1416567

[10] Suo Z, Shih CF, Varias AG. A theory for cleavage cracking in the presence of plastic flow. Acta Metallurgica et Materialia. 1993;**41**(5):1551-1557. DOI: 10.1016/0956-7151(93)90263-R

[11] Tane M, Okuda H, Tanaka F. Nanocomposite microstructures dominating anisotropic elastic modulus in carbon fibers. Acta Materialia. 2019; **166**:75-84. DOI: 10.1016/j. actamat.2018.12.029

[12] Okabe T, Takeda N. Size effect on tensile strength of unidirectional CFRP composites experiment and simulation. Composites Science and Technology. 2002;**62**(15):2053-2064. DOI: 10.1016/ S0266-3538(02)00146-X

[13] Van Den Heuvel PWJ, Van Der Bruggen YJW, Peijs T. Failure phenomena in multi-fibre model composites: Part 1. An experimental investigation into the influence of fibre spacing and fibre-matrix adhesion. Composites Part A Applied Science and Manufacturing. 1996;**27**(9):855-859. DOI: 10.1016/1359-835X(96)00023-1

[14] Van Dyke P, Hedgepeth JM. Stress concentrations from single-filament

failures in composite materials. Textile Research Journal. 1969;**39**(7):618-626. DOI: 10.1177/004051756903900702

[15] Nedele MR, Wisnom MR. Stress concentration factors around a broken fibre in a unidirectional carbon fibre-reinforced epoxy. Composites. 1994; **25**(7):549-557. DOI: 10.1016/0010-4361 (94)90183-X

[16] Nedele MR, Wisnom MR. Three-dimensional finite element analysis of the stress concentration at a single fibre break. Composites Science and Technology. 1994;**51**(4):517-524. DOI: 10.1016/0266-3538(94)90084-1

[17] Wisnom MR, Green D. Tensile failure due to interaction between fibre breaks. Composites. 1995;**26**(7): 499-508. DOI: 10.1016/0010-4361(95) 96807-I